Investigation of low-lying electric dipole strength in the semimagic nucleus ^{44}Ca

J. Isaak,[1,*] D. Savran,[2,3] M. Fritzsche,[1] D. Galaviz,[4] T. Hartmann,[1,†] S. Kamerdzhiev,[5,6] J. H. Kelley,[7,8] E. Kwan,[8,9] N. Pietralla,[1] C. Romig,[1] G. Rusev,[8,9] K. Sonnabend,[1] A. P. Tonchev,[8,9] W. Tornow,[8,9] and A. Zilges[10]

[1]*Institut für Kernphysik, Technische Universität Darmstadt, Schlossgartenstrasse 9, D-64289 Darmstadt, Germany*

[2]*ExtreMe Matter Institute EMMI and Research Division, GSI Helmholtzzentrum für Schwerionenforschung GmbH, Planckstraße 1, D-64291 Darmstadt, Germany*

[3]*Frankfurt Institute for Advanced Studies (FIAS), Ruth-Moufang-Strasse 1, D-60438 Frankfurt am Main, Germany*

[4]*Centro de Fisica Nuclear, University of Lisbon, P-1649-003 Lisbon, Portugal*

[5]*Institut für Kernphysik, Forschungszentrum Jülich, D-52425 Jülich, Germany*

[6]*Institute of Physics and Power Engineering, 249033 Obninsk, Russia*

[7]*Department of Physics, North Carolina State University, Raleigh, North Carolina 27695-8202, USA*

[8]*Triangle Universities Nuclear Laboratory, Durham, North Carolina 27708, USA*

[9]*Department of Physics, Duke University, Durham, North Carolina 27708-0308, USA*

[10]*Institut für Kernphysik, Universität zu Köln, Zülpicher Straße 77, D-50937 Köln, Germany*

(Received 21 November 2010; revised manuscript received 9 January 2011; published 7 March 2011)

The dipole-strength distribution in the semimagic nucleus ^{44}Ca has been measured up to 10 MeV excitation energy in photon-scattering experiments using bremsstrahlung and monoenergetic 100% linearly polarized photon beams. The combination of both measurements allows a clear determination of spin and parity quantum numbers of the excited states as well as absolute cross sections and transition probabilities. The results show that the majority of the dipole strength in ^{44}Ca below 10 MeV is due to $E1$ transitions while $M1$ strength plays only a minor role. The experimental results are compared to the strength in the neighboring doubly magic nuclei ^{40,48}Ca and to microscopic calculations within the extended theory of finite Fermi systems in order to investigate the evolution of the low-lying $E1$ strength in this isotopic chain. Both, experiment and calculations, show a nontrivial dependence of the total $E1$ strength as a function of the neutron number.

DOI: 10.1103/PhysRevC.83.034304 PACS number(s): 21.10.Hw, 21.10.Re, 21.60.Jz, 23.20.−g

I. INTRODUCTION

The major part of the electric-dipole ($E1$) excitation strength of atomic nuclei is located in the well-known isovector electric giant dipole resonance (IVGDR). The IVGDR was the first giant resonance discovered in atomic nuclei and has been studied extensively [1].

In the past decade the observation of additional low-lying strength superimposed on the low-energy tail of the IVGDR [2–7] has initiated the investigation of the $E1$ strength distributions in atomic nuclei in the energy region well below the IVGDR. In most medium- and heavy-mass nuclei, a concentration of $E1$ strength below or in the vicinity of the particle separation energies has been observed, which is usually denoted as pygmy dipole resonance (PDR). The interpretation of this new widespread excitation mode of atomic nuclei is a matter of ongoing discussion. Most microscopic models favor the picture of an oscillating neutron skin against a proton-neutron core (see Ref. [8] for a recent discussion). In that case, a dependence of the total strength of the PDR on the neutron excess should be expected and, thus, systematic investigation especially in isotopic and isotonic chains is a major tool in order to experimentally verify such a behavior.

Most of the available data on $E1$ strength in stable isotopes below the neutron-separation energy has been obtained using the experimental method of nuclear resonance fluorescence (NRF) [9]. Due to the low-momentum transfer of the photons nearly exclusively, dipole transitions are induced, i.e., in even-even nuclei selectively, $J^\pi = 1^\pm$ states are populated. Systematic surveys of (γ,γ') experiments have been performed in different mass regions [4,10–17]. The results show that the PDR exhausts up to about 1% of the energy weighted sum rule (EWSR) in the region below the neutron-separation energy. Generally, the strength of the PDR increases for heavier and more neutron rich nuclei. In unstable nuclei, $E1$ strength below the IVGDR has been studied using Coulomb excitation in inverse kinematics in the region of ^{132}Sn [7,18] and in ^{68}Ni [19]. In all cases a concentration of $E1$ strength above the neutron-separation energy carrying a few percent of the EWSR is reported. However, the sensitivity of the two experimental approaches (scattering real photons off stable nuclei and projectile-Coulomb excitation on exotic nuclei from radioactive ion beams) were restricted to partly different excitation energy regions, either to the energy range below the neutron-separation energy or, due to experimental details in most of the previous relativistic Coulomb excitation experiments, to energies above the separation energy. This fact prohibits at this point a meaningful global comparison of the observations from both techniques. At least in the few cases where the same excitation energy range in neighboring isotopes was covered, the data obtained with

*jisaak@ikp.tu-darmstadt.de

†Present address: Philipp-Röth-Weg 28, 64295 Darmstadt.

both methods indicate a corresponding enhancement of $E1$ strength [18].

In the medium-mass region, the Ca isotopic chain is very well suited to study the influence of the proton to neutron ratio on the low-lying $E1$ strength, since one finds stable nuclei with N/Z ranging from 1.0 (^{40}Ca) to 1.4 (^{48}Ca). NRF experiments on the two doubly magic nuclei ^{40,48}Ca showed a huge difference of about one order of magnitude in the integrated $E1$ strength up to S_n [20,21]. To investigate the evolution within the isotopic chain we have performed an NRF experiment on ^{44}Ca using bremsstrahlung at the Darmstadt High-Intensity Photon Setup (DHIPS) at the S-DALINAC [22]. First results of the experiment have been published in a previous Letter [12], together with calculations within the extended theory of finite Fermi systems (ETFFS). A nontrivial dependence of the total strength located below 10 MeV has been observed for both experiment and theory. Since in experiments with unpolarized bremsstrahlung parity determinations in the PDR region are difficult (see [23,24]) we have performed an additional NRF experiment using polarized photons at the High-Intensity γ-ray Source (HIγS) facility [25] in order to verify the $E1$ character of the observed dipole strength and identify $M1$ contributions.

In this paper we report on the experimental results. The data will be compared to recent calculations in the ETFFS [26]. In the next section the experimental setups at DHIPS and HIγS are introduced briefly. In Sec. III, the data analysis is described, and Sec. IV presents the results and a discussion.

II. EXPERIMENTAL SETUPS

At DHIPS [22] photons are produced via bremsstrahlung by stopping completely the intense electron beam delivered by the injector of the electron accelerator S-DALINAC in a thick copper radiator. The continuous photon beam is collimated to a size of about 2.5 cm diameter at the target position by a copper collimator system. Large volume high-purity germanium (HPGe) detectors are used to detect the scattered photons at different angles (90° and 130°) with respect to the beam axis. The detectors are heavily shielded against background stemming from the radiator and are additionally equipped with Bismuth germanate (BGO) active Compton-surpression shields. The ^{44}Ca target consisted of 1.083 g of CaO_3 enriched to 97.1% in the isotope of interest. For energy and photon-flux calibrations 1.293 g of ^{11}B were added to the target. Measurements at two different end-point energies of $E_0 = 6.3$ MeV and $E_0 = 9.9$ MeV have been performed in order to identify transitions to excited states and feeding contributions. Table I summarizes the experimental parameters for the measurements at DHIPS.

TABLE I. Parameters of the experiments at DHIPS.

End-point energy	(MeV)	9.9	6.3
Measuring time	(h)	69.5	20.5
Electron beam current	(μA)	35.5	
Element mass ^{44}Ca	(g)	1.052	
Element mass ^{11}B	(g)	1.293	

Figure 1 shows a sample spectrum in the energy region 4–9 MeV for the measurement at a bremsstrahlung end-point energy of $E_0 = 9.9$ MeV. An accumulation of large peaks stemming from the decay of excited states of ^{44}Ca is visible in the region 5–8 MeV. Peaks originating from ^{11}B are marked with an asterisk.

The second NRF experiment was performed at the HIγS at Duke University [25]. The photon beam is produced via intercavity laser Compton backscattering (LCB) of a free-electron laser (FEL) beam with relativistic electrons in a storage ring. The FEL is powered by the same electron beam which is used for the scattering process. In comparison to other LCB facilities with external lasers a high photon flux is achieved, which is sufficient to perform NRF experiments with reasonable statistics within a few hours of beam time.

Due to the polarization conservation of the Compton scattering the produced photon beam is linearly polarized to nearly 100% in the horizontal direction. A lead collimator system in front of the NRF setup about 60 m downstream of the collision point is used to define the size of the beam spot at the NRF target position. Since the energy of the scattered photons strongly depends on the scattering angle, the collimator also

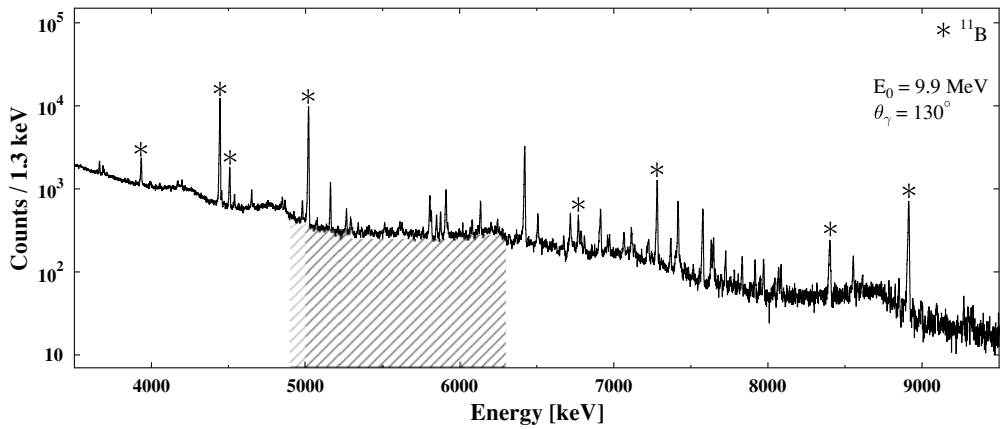

FIG. 1. The γ-ray spectrum of ^{44}Ca measured at $E_0 = 9.9$ MeV at DHIPS. Peaks resulting from transitions in ^{11}B and their escape lines are marked with an asterisk. The shaded area highlights the energy region shown in Fig. 2.

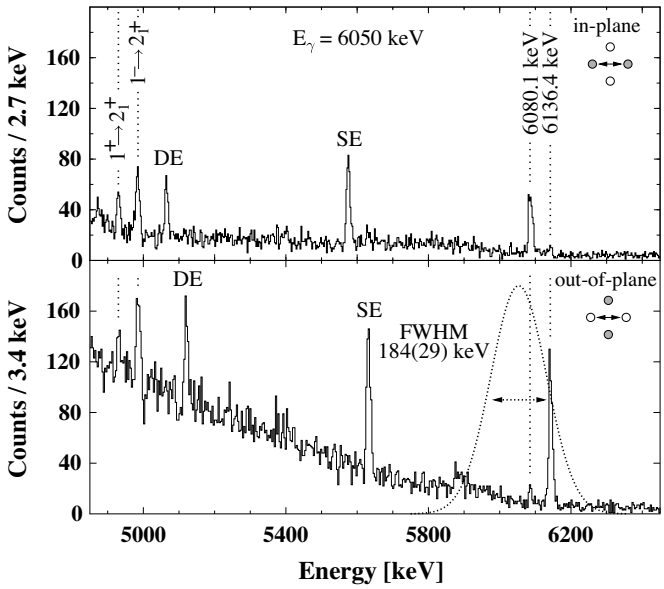

FIG. 2. Spectra measured at HIγS parallel (upper panel) and perpendicular (lower panel) to the polarization plane at a photon beam energy of 6050 keV. Single-escape (SE) and double-escape (DE) lines are marked. The incident photon intensity profile is shown by a dashed curve. Besides the decays to the ground state at 6080 and 6136 keV, peaks are also observed at 4923 and 4979 keV, respectively, corresponding to transitions to the first excited state.

defines the degree of monochromacy of the photon beam. For the present experiment a collimator with a diameter of 1 in. was used which yielded a photon beam with about a 3% energy spread (full width at half maximum).

For the detection of the scattered photons, four HPGe clover detectors were positioned at different angles perpendicular to the incoming beam. This is sufficient to determine the parity of the excited states (see Sec. III). The target consisted of 1.693 g of CaO_3 enriched to 95.8% in ^{44}Ca. Because of the small energy spread of the photon beam, measurements at eight energy configurations between 6 and 10 MeV have been taken to investigate as many excited states in as wide of an energy range as possible.

In Fig. 2, two sample spectra in the energy region from 4.8 to 6.4 MeV for the measurement at the centroid beam energy of 6050 keV are shown. The upper spectrum was measured parallel to, and the lower one perpendicular to the polarization plane, respectively. In addition to the ground-state transitions of the excited states, peaks corresponding to transitions to the first excited state in ^{44}Ca are also visible. Figure 2 shows also the intensity profile of the incident photon beam (dashed curve). Due to the narrow photon spectrum only levels in a limited energy region are excited and transitions to the ground state can easily be distinguished from decays to excited states.

III. DATA ANALYSIS

One of the advantages of the NRF method is the fact that intrinsic properties of the excited states such as spins, parities, and absolute transition probabilities can be determined in a model-independent way. These quantities are analytically linked to direct observables such as the cross sections, the angular distribution, or the polarization asymmetries (see, for example, Refs. [9,27] for a detailed description of the method).

The determined peak area A_i in a spectrum (as shown in Fig. 1) corresponding to the decay of a photoexcited state is proportional to the integrated scattering cross section $I_{i,0}$, the angular distribution $W_i(\theta, \phi)$, photon flux N_γ, and detection efficiency ε,

$$A_i \propto I_{i,0} W_i(\theta, \phi) N_\gamma(E_i) \varepsilon(E_i). \quad (1)$$

Another advantage of NRF experiments using (continuous-energy) bremsstrahlung over those with a strongly varying intensity profile is the possibility to measure integrated cross sections relative to a calibration standard. In our case we used the ^{11}B(γ,γ') reaction to determine $N_\gamma\varepsilon$ for the energies of the excited states in ^{11}B with well-known excitation cross sections [28]. The ^{44}Ca target is sandwiched between two ^{11}B targets, so both reactions are measured simultaneously. Therefore, the relevant normalization factors are the same for both reactions. The smooth energy dependence of the bremsstrahlung spectrum allows an easy interpolation of $N_\gamma\varepsilon$ between the calibration points at the energies of the excited states of ^{11}B. This yields in an absolute normalization of $N_\gamma\varepsilon$ and thus allows the determination of absolute cross sections with low systematic errors.

In scattering experiments with real photons the relation between the integrated elastic scattering cross section $I_{i,0}$ and the ground-state decay width Γ_0 is given by [29]

$$I_{i,0} = \pi^2 \left(\frac{\hbar c}{E_i}\right)^2 g \frac{\Gamma_0^2}{\Gamma} \quad (2)$$

with Γ being the total width and E_i the energy of the excited state [9]. The spin factor $g = (2J_i + 1)/(2J_0 + 1)$ is determined by the spins of the ground state J_0 and of the excited state J_i. As mentioned above, $I_{i,0}$ can be determined relative to well-known excitation cross sections in ^{11}B. In order to extract the ground-state decay width, which is needed to calculate the excitation strength [see Eqs. (6) and (7) below], the spin J_i and the branching ratio Γ_0/Γ need to be known.

The spin of an excited state can be determined in NRF experiments by measuring the angular distribution of the elastically scattered photons. The expectation value for the ratio of $W(\theta_\gamma)$ at the two detector angles realized at DHIPS is $W(90°)/W(130°) = 0.7$ and $W(90°)/W(130°) = 2.2$ for the spin sequence $0 \to 1 \to 0$ and $0 \to 2 \to 0$ in even-even nuclei, respectively. The large difference for the two spin sequences usually allows spin assignments for weakly excited states as well. Figure 3 shows the measured ratios $W(90°)/W(130°)$ for all observed ground-state transitions in ^{44}Ca. The results show that above 3.5 MeV for all states $J = 1$ could be assigned unambiguously.

The strength-selective method of NRF preferentially populates dipole excitations with a large decay width to the ground state. Consequently, the nuclear states observed in NRF experiments usually decay predominantly to the ground state. In several cases decay branches to lower-lying excited states have been observed. Even though the high peak density in

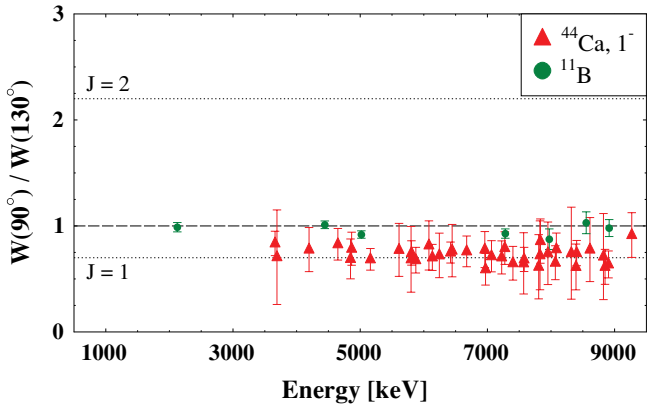

FIG. 3. (Color online) The ratio $W(90^\circ)/W(130^\circ)$ for all measured transitions. All previously unknown states can clearly be assigned to $J = 1$. The circles mark corresponding data for the calibration standard ^{11}B which shows a nearly isotropic NRF distribution due to the nonzero $J_0^\pi = \frac{3}{2}^-$ ground-state spin.

experiments with continuous photon sources makes it difficult, measurements at different end-point energies have been performed at DHIPS to identify transitions stemming from inelastic reactions. The experiments using the monoenergetic photon beam at HIγS have a higher sensitivity to transitions to excited states, because they do not suffer from the high background usually present at low energies in experiments using bremsstrahlung. Hence, transitions to excited states can most clearly be identified from the HIγS data as shown for one example in Fig. 2. For the determination of the decay branching ratios the relative efficiencies at the transition energies are needed, which were simulated using the Monte Carlo code Geant4 [30]. It has been shown that the simulation of relative efficiencies can be done within Geant4 with accuracies of less than 2% [31], which is more than sufficient for our needs. In all cases where in both experiments no transition to an excited state is observed, $\Gamma_0/\Gamma = 1$ is assumed in order to calculate Γ_0 from the integrated cross section. Since small decay branches stay unobserved, this assumption could lead to a slight underestimation of the ground-state decay width. On the other hand, in that case also the feeding of the lower-lying states could not be correctly accounted for, which would lead to an overestimation of their cross sections. However, the comparison of the results for the measurement at DHIPS with the lower end-point energy shows no significant differences to the results obtained with a higher end point and neglecting feeding. This observation indicates that systematical errors due to incorrect treatment of the decay intensity between highly excited states can be neglected within the accuracy achieved in our experiments.

A great advantage of NRF experiments using polarized photons at HIγS is the possibility to determine parity quantum numbers of excited $J = 1$ states with excellent accuracy [32–34]. In the case of elastic resonant photon scattering the angular distribution for the spin sequence $0^+ \xrightarrow{\vec{\gamma}} 1^\pi \xrightarrow{\gamma'} 0^+$ in even-even nuclei is given by [35]

$$W(\vartheta, \varphi) = \tfrac{3}{2} + \tfrac{3}{4}(1 - \cos^2\vartheta)(\pi \cos 2\varphi - 1). \qquad (3)$$

The angle φ is defined as the angle between the reaction plane (defined by the momentum vectors of the incident and scattered photons) and the polarization plane (defined by the electric field and momentum vectors of the incoming photon) while ϑ is the polar scattering angle. The parameter π depends on the parity quantum number of the excited states and is -1 for negative parity and $+1$ for positive parity. Since the angular distribution for $E1$ and $M1$ transitions shows minima and maxima at perpendicular directions with respect to the polarization plane it is sufficient to measure the intensity of the scattered photons at $\varphi = 0^\circ$ and $\varphi = 90^\circ$. The maximum analyzing power Σ is achieved for $\vartheta = 90^\circ$:

$$\Sigma = \frac{W(90^\circ, 0^\circ) - W(90^\circ, 90^\circ)}{W(90^\circ, 0^\circ) + W(90^\circ, 90^\circ)} = \pi = \begin{cases} +1 & \text{for } J^\pi = 1^+ \\ -1 & \text{for } J^\pi = 1^- \end{cases}. \qquad (4)$$

Hence, the HPGe clover detectors are surrounding the ^{44}Ca target at the polar scattering angle $\vartheta = 90^\circ$ and are positioned parallel to the polarization plane (azimuthal scattering angles $\varphi = 0^\circ$ and $\varphi = 180^\circ$, respectively) and perpendicular to it (azimuthal scattering angles $\varphi = 90^\circ$ and $\varphi = 270^\circ$, respectively). For the determination of the parities of excited states the asymmetry ϵ is defined by means of the efficiency-corrected peak areas parallel ($N_\parallel$) and perpendicular ($N_\perp$) to the polarization plane in the measured spectra:

$$\epsilon = \frac{N_\parallel - N_\perp}{N_\parallel + N_\perp} = Q\Sigma. \qquad (5)$$

The experimentally observed asymmetry is somewhat smaller than ± 1.0 due to the finite size of the target and the finite solid angles of the detectors. This effect is described by the experimental sensitivity Q in Eq. (5) which has been extracted by fitting on the experimental data. Its value is $Q = 0.9$ in the present setup. The determined asymmetries are shown in Fig. 4.

Due to the high polarization sensitivity of our setup, the γ-ray count rates in the disfavored direction of observation can be small. Statistical fluctuations of the background can then lead in a simple background subtraction applied here to quoted

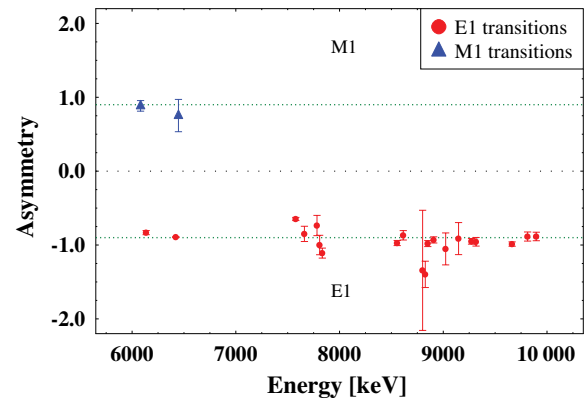

FIG. 4. (Color online) Asymmetries observed in ^{44}Ca. The average values for the measured asymmetries are $\epsilon = -0.9$ for $E1$ transitions and $\epsilon = +0.9$ for $M1$ transitions.

absolute asymmetry values $|\epsilon| > 1$. The clean assignment of parity quantum numbers from our data is not, however, affected by this and a substantially more involved treatment of uncertainties is unnecessary.

As already mentioned above, another advantage of the HIγS facility is the sensitivity for the observation and identification of transitions to lower-lying excited states. Due to the narrow intensity distribution of the γ-ray beam, only states in a small energy range are excited. Thus, peaks in the region below the beam energy are stemming either from the detector response, background, or inelastic scattering processes, as shown in Fig. 2. The two lower peaks marked by the vertical dashed lines result from the transitions of the two $J = 1$ states at 6080.1 and 6136.4 keV to the 2_1^+ state with an energy of $E_{2_1^+} = 1157.0$ keV. In addition to the decays to the 2_1^+ state, transitions to the 0_2^+ state at $E_{0_2^+} = 1883.5$ keV have been observed in a few cases. Using the spectra measured at HIγS the branching ratios to these states can be determined with good accuracy. In the experiment using continuous-energy bremsstrahlung a wide energy region up to the end-point energy is covered. Hence, the peak density in the obtained spectra is relatively high and consequently, the identification of transitions to excited states is often complicated.

Combining the results obtained at DHIPS using bremsstrahlung and HIγS using LCB photons thus allows a determination of cross sections, spin and parity quantum numbers, and branching ratios of the excited states. With these observables it is possible to calculate the ground-state decay widths Γ_0 and herewith the $B(E1)$ and $B(M1)$ transition strengths, given by

$$\frac{B(E1)\uparrow}{[e^2\ \mathrm{fm}^2]} = 9.554 \times 10^{-4} g \frac{\Gamma_0}{[\mathrm{meV}]} \left(\frac{[\mathrm{MeV}]}{E_j}\right)^3, \quad (6)$$

$$\frac{B(M1)\uparrow}{[\mu_N^2]} = 8.641 \times 10^{-2} g \frac{\Gamma_0}{[\mathrm{meV}]} \left(\frac{[\mathrm{MeV}]}{E_j}\right)^3. \quad (7)$$

In the following section the results are presented and discussed in comparison to theoretical calculations in the ETFFS model.

IV. RESULTS AND DISCUSSION

In total, 52 excited $J = 1$ states have been observed. The $J = 1$ state at 3661.5(2) keV was already known, while the spin for three further known low-lying states have been determined to be $J = 1$. Moreover, the spin quantum number for the state at 4196.3(3) keV previously assigned to be $J^\pi = 2^+$ (see [36]) has been corrected to $J = 1$.

Unfortunately not all energy regions could be covered in the experiments at HIγS due to lack of beam time. Out of all the states investigated at HIγS, 20 negative and 3 positive-parity quantum numbers have been assigned. The positive-parity states show rather small transition strengths to the ground state compared to the other excitations, which proves that the majority of the observed dipole strength is due to $E1$.

Because of the modest energy resolution for the scattered photons of about 12 keV at the HIγS setup, the $J = 1$ states at 7572.0(5) and 7578.9(3) keV, which were observed at DHIPS, could not be identified, separately. The transition width Γ_i for the higher-lying state is approximately five times bigger than the lower-lying one as determined at DHIPS. The experimental asymmetry for the combined peak at 7578.9(3) keV has been

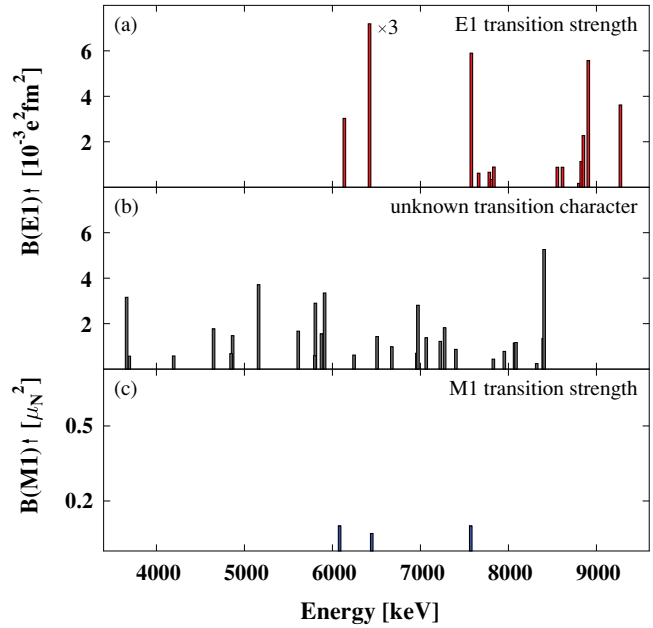

FIG. 5. (Color online) The $E1$ and $M1$ strength distributions are shown in (a) and (c), respectively. The transitions where no character has been assigned are plotted in $B(E1)\uparrow$ units in (b). For a better comparability between the $E1$ and $M1$ strengths the three plots have the same scale. The observed $M1$ strength is almost negligible compared to the total dipole strength.

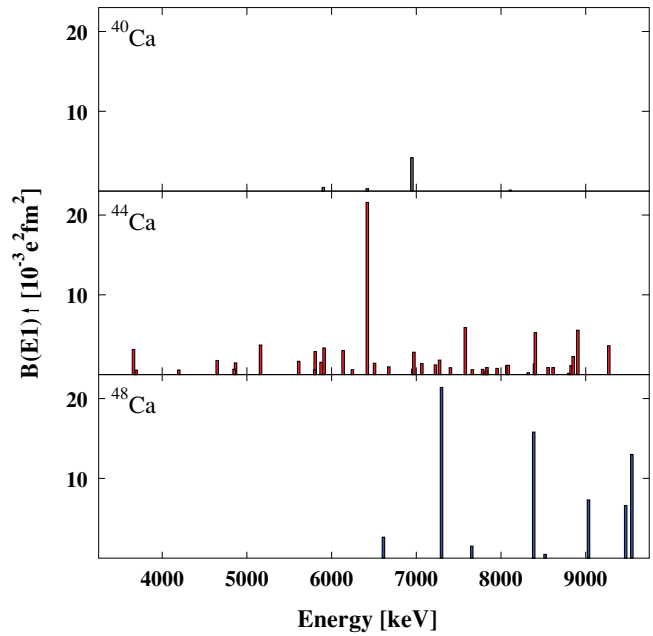

FIG. 6. (Color online) $B(E1)$ strength distribution in the Ca isotopes ^{40,44,48}Ca. All experiments have been performed up to 9.9 MeV.

TABLE II. Determined properties of observed excited states in ^{44}Ca (g.s. denotes ground state). For details see the text.

E_{level} (keV)	E_γ (keV)	E_{final} (keV)	ϵ	J^π ($\hbar$)	I_γ (%)	Γ_i (eV)	$B(E1)\uparrow$ ($10^{-3}e^2$ fm^2]	$B(M1)\uparrow$ (μ_N^2)
3661.5(2)[a]	3661.3(2)	g.s.		$1^\pm$	100.0(19)[b]	0.054(13)	3.16(76)	0.29(7)
	2504.39(6)	1157.0			10.7(9)[b]	0.0058(15)		
	1777.973(20)	1883.5			34.8(8)[b]	0.0188(46)		
	1005.0(9)	2657.0			0.48[b]	0.00026(7)		
	353.67(25)	3307.87			0.3(2)[b]	0.0002(1)		
3691.7(4)	3691.5(4)	g.s.		$1^\pm$	100	0.010(4)	0.57(21)	0.05(2)
4196.3(3)[a]	4196.1(3)	g.s		$1^{\pm c}$	100	0.015(3)	0.58(12)	0.05(1)
4649.5(1)	4649.2(1)	g.s.		$1^\pm$	100	0.062(11)	1.77(32)	0.16(3)
4848.4(2)	4848.1(2)	g.s.		$1^\pm$	100	0.027(6)	0.68(15)	0.06(1)
4866.0(4)[a]	4865.7(4)	g.s.		$1^\pm$	100(27)	0.059(16)	1.47(41)	0.13(4)
	2982.3(3)	1883.5			79(27)	0.047(21)		
5161.0(3)[a]	5160.7(3)	g.s.		$1^\pm$	100	0.178(19)	3.71(41)	0.34(4)
5611.6(3)	5611.2(3)	g.s.		$1^\pm$	47(21)	0.103(20)	1.67(32)	0.15(3)
	4454.1(8)	1157.0			100(21)	0.22(11)		
5800.6(2)[a]	5800.2(2)	g.s.		$1^{\pm d}$	100	0.040(12)	0.59(17)	0.05(2)
5806.3(1)	5805.9(1)	g.s.		$1^\pm$	100	0.198(25)	2.90(36)	0.26(3)
5875.8(2)	5875.4(2)	g.s.		$1^\pm$	100	0.110(15)	1.55(21)	0.65(9)
5911.1(2)	5910.7(2)	g.s.		$1^\pm$	100	0.241(59)	3.35(82)	0.30(7)
6080.6(14)	6080.1(14)	g.s.	0.88(7)	1^+	100(7)	0.109(29)		0.13(5)
	4925.3(8)	1157.0	0.06(17)		41(7)	0.045(15)		
	4199.5(5)	1883.5	1.16(30)		62(12)	0.068(22)		
6136.9(3)	6136.4(3)	g.s.	−0.83(3)	1^-	100(5)	0.245(39)	3.03(65)	
	4978.5(5)	1157.0	−0.05(8)		46(7)	0.113(29)		
6245.5(3)	6245.0(3)	g.s.		$1^\pm$	100	0.053(12)	0.62(14)	0.06(1)
6422.1(1)	6421.6(1)	g.s.	−0.89(1)	1^-	100(1)	1.99(21)	21.6(32)	
	5263.8(7)	1157.0	−0.14(7)		5.5(7)	0.110(18)		
	4539.9(7)	1883.5	−1.24(25)		5.2(7)	0.104(18)		
6446.8(8)	6446.3(8)	g.s.	0.75(22)	1^+	100(10)	0.052(14)		0.05(2)
	5288.0(17)	1157.0	0.08(37)		50(14)	0.026(10)		
6507.1(5)	6506.6(5)	g.s.		$1^\pm$	100	0.137(30)	1.43(31)	0.13(3)
6675.4(2)	6674.9(2)	g.s.		$1^\pm$	100	0.102(17)	0.98(17)	0.09(2)
6960.7(6)	6960.1(6)	g.s.		$1^\pm$	100	0.082(16)	0.70(13)	0.06(1)
6972.1(2)	6971.5(2)	g.s.		$1^\pm$	52(15)	0.332(56)	2.81(47)	1.17(20)
	5815.0(5)	1157.0			100(15)	0.64(21)		
7065.9(9)	7065.3(9)	g.s.		$1^\pm$	100	0.170(29)	1.38(24)	0.13(2)
7226.0(3)	7225.4(3)	g.s.		$1^\pm$	100	0.161(27)	1.22(21)	0.11(2)
7275.1(9)	7274.5(9)	g.s.		$1^\pm$	100	0.245(40)	1.82(30)	0.17(3)
7403.0(8)	7402.3(8)	g.s.		$1^\pm$	100	0.123(23)	0.87(16)	0.08(2)
7572.0(5)	7571.3(5)	g.s.		1^+	100	0.173(39)		0.10(2)
7578.9(3)	7578.2(3)	g.s.	−0.65(2)	1^-	100	0.90(11)	5.90(75)	
7662.1(6)	7661.4(6)	g.s.	−0.85(10)	1^-	100	0.098(30)	0.62(19)	
7783.3(10)	7782.6(10)	g.s.	−0.74(14)	1^-	100	0.108(33)	0.66(20)	
7808.9(16)	7808.2(16)	g.s.	−1.00(13)	1^-	100	0.057(18)	0.34(11)	
7828.8(12)	7828.1(12)	g.s.		$1^\pm$	100	0.074(24)	0.44(15)	0.04(1)
7834.8(8)	7834.0(8)	g.s.	−1.11(7)	1^-	100	0.150(35)	0.89(21)	
7953.4(5)	7952.6(5)	g.s.		$1^\pm$	50(23)	0.136(45)	0.78(26)	0.07(2)
	5293.8(14)	2657.0			50(23)	0.136(65)		
8070.2(7)	8069.4(7)	g.s.		$1^\pm$	100	0.210(39)	1.15(21)	0.10(2)
8086.0(7)	8085.2(7)	g.s.		$1^\pm$	100	0.215(39)	1.17(21)	0.11(2)
8321.5(16)	8320.7(16)	g.s.		$1^\pm$	100	0.048(21)	0.24(11)	0.02(1)
8395.3(4)	8394.4(4)	g.s.		$1^\pm$	100	0.278(65)	1.35(32)	0.12(3)
8405.4(17)	8404.5(17)	g.s.		$1^\pm$	100	1.09(16)	5.26(77)	0.48(7)
8556.7(8)	8555.8(8)	g.s.	−0.97(4)	1^-	100	0.193(79)	0.88(36)	
8615.2(12)	8614.3(12)	g.s.	−0.87(6)	1^-	100	0.197(60)	0.88(27)	
8801.9(29)	8800.9(29)	g.s.	−1.34(81)	1^-	100	0.041(22)	0.17(9)	
8827.6(14)	8826.6(14)	g.s	−1.40(18)	1^-	89(23)	0.27(11)	1.13(62)	

TABLE II. (*Continued*.)

E_{level} (keV)	E_γ (keV)	E_{final} (keV)	ϵ	J^π ($\hbar$)	I_γ (%)	Γ_i (eV)	$B(E1)\uparrow$ ($10^{-3}e^2$ fm^2]	$B(M1)\uparrow$ (μ_N^2)
	6944.6(18)	1883.5	−1.24(20)		100(14)	0.31(14)		
8851.7(7)	8850.7(7)	g.s.	−0.98(4)	1^-	100(6)	0.55(12)	2.27(66)	
	7692.9(18)	1157.0	−0.79(29)		19(8)	0.105(49)		
8908.8(7)	8907.8(7)	g.s.	−0.93(4)	1^-	100	1.37(23)	5.57(93)	
9024.1(20)	9023.1(20)	g.s.	−1.05(22)	1^-	100			
9148.4(24)	9147.4(24)	g.s.	−0.91(22)	1^-	100			
9273.6(8)	9272.5(8)	g.s.	−0.95(4)	1^-	100	0.433(96)	3.62(81)	
9317.2(10)	9316.1(10)	g.s.	−0.96(5)	1^-	100			
9664.8(7)	9663.7(7)	g.s.	−0.99(3)	1^-	100(6)			
	8508.5(33)	1157.0	0.13(23)		17(8)			
9814.1(11)	9812.9(11)	g.s.	−0.89(6)	1^-	100			
9898.2(10)	9897.0(10)	g.s.	−0.88(6)	1^-	100			

[a]Excited state already known in [36].
[b]Relative strength in [36].
[c]Assigned spin in [36]: $J = 2^+$.
[d]Spin unknown in [36].

determined to be $\epsilon = -0.65(2)$ (which significantly deviates from the expectation value of $|\bar{\epsilon}| = 0.90(2)$ for a single transition). Assuming the parity of the weaker state to be positive while the other state has negative parity, the combined expected asymmetry for the sum of both states is estimated to be $\epsilon_{sum} = -0.61(6)$. This is in good agreement with the experimental value, thus, the assignments $J^\pi = 1^+$ to the level at 7572.0(5) keV, and $J^\pi = 1^-$ to the level at 7578.9(3) keV are justified.

The experimental asymmetries ϵ, relative strengths I_γ, decay widths Γ_i, and the corresponding transition strengths $B(E1)$ and $B(M1)$, respectively, are summarized in Table II. For all transitions where no electromagnetic character has been determined, both possible excitation strengths are given.

The strength distribution in the region of 3–10 MeV in ^{44}Ca is shown in Fig. 5 separately for $E1$, $M1$, and undetermined multipolarity. The contribution of $M1$ in the regions covered at HIγS to the total dipole strength is less than 3%. Therefore, an assumption of predominant $E1$ character for the undetermined dipole strength seems to be well justified.

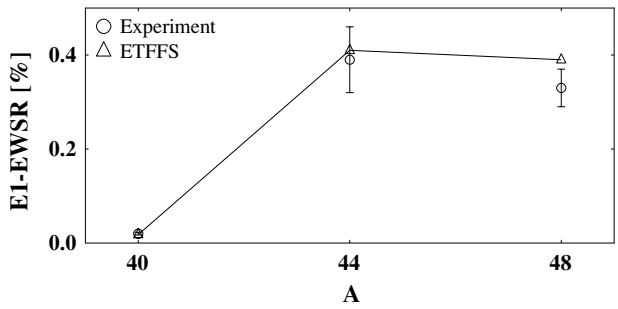

FIG. 7. Comparison of the experimental results with ETFFS (solid lines) calculations. The evolution of the energy weighted electric-dipole strength in the energy region from 5 to 10 MeV is shown for the Ca isotopes. Within the experimental errors the ETFFS reproduces the experimental values.

As mentioned in the Introduction, NRF experiments have previously been performed in the neighboring isotopes ^{40}Ca and ^{48}Ca [20,21]. Figure 6 shows the $B(E1)$ strength distributions for all three Ca isotopes in the investigated energy region up to 10 MeV. In ^{40}Ca almost no $E1$ strength is observed, as expected from an $N = Z$ nucleus. In ^{44}Ca and ^{48}Ca a fragmented pattern of $E1$ strength is observed, while in ^{44}Ca the fragmentation is much stronger and the strength is shifted to lower excitation energies. The integrated strength for ^{40,44,48}Ca up to the experimental limit of 10 MeV is shown in Fig. 7 as a fraction of the EWSR. The enhancement of the low-lying strength going from ^{40}Ca to ^{44}Ca is obvious, however no further increase is observed in ^{48}Ca. Also shown in Fig. 7 are the results for calculations within the ETFFS. As described in [12,26] these microscopic calculations are able to reproduce the complex pattern of the measured $B(E1)$ strength distribution shown in Fig. 6 by including coupling to complex configurations and the single-particle continuum as well as pairing. In the summed $B(E1)$ strength up to 10 MeV the new ETFFS calculations [26] are in good agreement with the experimental values and show the same nontrivial dependence on the neutron excess. However, this nontrivial dependence may be due to the experimental limitations to $E_\gamma < 10$ MeV. Actually, the ETFFS calculations for ^{48}Ca show additional strength located around 11 MeV which, when included in the summed strength, leads to an enhancement of the PDR with increasing neutron number.

V. CONCLUSIONS

In conclusion, the dipole-strength distribution in the semimagic nucleus ^{44}Ca was measured below the particle threshold in NRF experiments at DHIPS and in addition, parity assignments for 23 $J = 1$ states have been obtained at HIγS. The fraction of identified $M1$ strength up to 10 MeV is less than 3% of the total dipole strength and thus can be neglected in the

integrated dipole strength. The results on ^{44}Ca have been compared to experimental data from other NRF experiments on the doubly magic nuclei ^{40,48}Ca [20,21]. In all cases the experiments have been performed up to 9.9 MeV. No simple relation of the exhaustion of the EWSR depending on the N/Z ratio has been observed. Current calculations by means of the ETFFS [26] are in good agreement with the experimental results.

However, the theoretical calculation for ^{48}Ca shows an accumulation of electric-dipole strength in the region of 11 MeV where NRF measurements cannot be performed due to the neutron separation threshold at 9.94 MeV. The predicted additional $E1$ strength could lead to a dependence of the low-lying $E1$ strength on the neutron excess. Therefore, additional experiments, e.g., through (γ,n) reactions using LCB or tagged photons [37], in the energy region above the particle threshold are mandatory in order to finally conclude on the dependence of the low-lying $E1$ strength on the neutron number in the Ca isotopic chain.

As in most other works on the PDR the total low-lying $E1$ strength has been assigned to the PDR strength, even though part of it may be due to the contributions of the low-energy tail of the IVGDR. However, without additional experimental observables it is not possible to distinguish between these two contributions. Thus, in the comparison to the ETFFS also in the calculation, the total $E1$ strength has been used, although differences in the shapes of the involved transition densities of the excited states are observed [26].

In order to get a deeper insight into the underlying structure of the $E1$ strength (e.g., on the shape of neutron and proton transition densities), experiments using experimental probes other than photons are of high importance. The method of $(\alpha,\alpha'\gamma)$ coincidence experiment [38] has recently been used to investigate particle bound $E1$ strength in different mass regions in order to study the structure of the single excitations [39–41].

The results show that different structures are involved. Preliminary results from a ^{48}Ca$(\alpha,\alpha'\gamma)$ experiment point to a similar situation in ^{48}Ca [42]. These experiments will help to study and pin down the nature of the $E1$ strength and are, therefore, as equally important as the systematic investigation presented in this paper.

ACKNOWLEDGMENTS

We thank the S-DALINAC group as well as the staff at the HIγS facility for their support during the beam times. We also thank M. Babilon, S. Volz, and W. Bayer for their help conducting the experiment at the DHIPS setup. This work was supported by the Deutsche Forschungsgemeinschaft (Grants No. SFB 634 and No. Zi 510/4-1), the Helmholtz Alliance Program of the Helmholtz Association (Contract No. HA216/EMMI "Extremes of Density and Temperature: Cosmic Matter in the Laboratory"), and by the LOEWE Program of the State of Hesse (Helmholtz International Center for FAIR). This research was also supported by DOE Grants No. DE-FG02-97ER41033 and No. DE-FG02-97ER41042, DFG Grant No. 436RUS113/994/0-1, and RFBR Grant No. 09-02-91352NNIO_a.

[1] M. N. Harakeh and A. van der Woude, *Giant Resonances* (Oxford University Press, USA, 2001).
[2] G. A. Bartholomew, E. D. Earle, A. J. Ferguson, J. W. Knowles, and M. A. Lone, Adv. Nucl. Phys. **7**, 229 (1973).
[3] R.-D. Herzberg *et al.*, Phys. Lett. B **390**, 49 (1997).
[4] K. Govaert, F. Bauwens, J. Bryssinck, D. De Frenne, E. Jacobs, W. Mondelaers, L. Govor, and V. Y. Ponomarev, Phys. Rev. C **57**, 2229 (1998).
[5] A. Zilges, M. Babilon, T. Hartmann, D. Savran, and S. Volz, Prog. Part. Nucl. Phys. **55**, 408 (2005).
[6] T. Aumann, Eur. Phys. J. A **26**, 441 (2005).
[7] P. Adrich *et al.* (LAND-FRS Collaboration), Phys. Rev. Lett. **95**, 132501 (2005).
[8] N. Paar, D. Vretenar, E. Khan, and G. Colo, Rep. Prog. Phys. **70**, 691 (2007).
[9] U. Kneissl, H. H. Pitz, and A. Zilges, Prog. Part. Nucl. Phys. **37**, 349 (1996).
[10] A. Zilges, S. Volz, M. Babilon, T. Hartmann, P. Mohr, and K. Vogt, Phys. Lett. B **542**, 43 (2002).
[11] N. Ryezayeva, T. Hartmann, Y. Kalmykov, H. Lenske, P. von Neumann-Cosel, V. Y. Ponomarev, A. Richter, A. Shevchenko, S. Volz, and J. Wambach, Phys. Rev. Lett. **89**, 272502 (2002).
[12] T. Hartmann, M. Babilon, S. Kamerdzhiev, E. Litvinova, D. Savran, S. Volz, and A. Zilges, Phys. Rev. Lett. **93**, 192501 (2004).
[13] S. Volz, N. Tsoneva, M. Babilon, M. Elvers, J. Hasper, R.-D. Herzberg, H. Lenske, K. Lindenberg, D. Savran, and A. Zilges, Nucl. Phys. A **779**, 1 (2006).
[14] R. Schwengner *et al.*, Phys. Rev. C **76**, 034321 (2007).
[15] R. Schwengner *et al.*, Phys. Rev. C **78**, 064314 (2008).
[16] D. Savran, M. Fritzsche, J. Hasper, K. Lindenberg, S. Müller, V. Y. Ponomarev, K. Sonnabend, and A. Zilges, Phys. Rev. Lett. **100**, 232501 (2008).
[17] N. Benouaret *et al.*, Phys. Rev. C **79**, 014303 (2009).
[18] A. Klimkiewicz *et al.*, Phys. Rev. C **76**, 051603 (2007).
[19] O. Wieland *et al.*, Phys. Rev. Lett. **102**, 092502 (2009).
[20] T. Hartmann, J. Enders, P. Mohr, K. Vogt, S. Volz, and A. Zilges, Phys. Rev. Lett. **85**, 274 (2000); **86**, 4981 (2001).
[21] T. Hartmann, J. Enders, P. Mohr, K. Vogt, S. Volz, and A. Zilges, Phys. Rev. C **65**, 034301 (2002).
[22] K. Sonnabend *et al.*, Nucl. Instrum. Methods A (accepted for publication).
[23] C. Hutter *et al.*, Nucl. Instrum. Methods A **489**, 247 (2002).
[24] M. A. Büssing, M. Elvers, J. Endres, J. Hasper, A. Zilges, M. Fritzsche, K. Lindenberg, S. Müller, D. Savran, and K. Sonnabend, Phys. Rev. C **78**, 044309 (2008).
[25] H. R. Weller, M. W. Ahmed, H. Gao, W. Tornow, Y. K. Wu, M. Gai, and R. Miskimen, Prog. Part. Nucl. Phys. **62**, 257 (2009).
[26] G. Tertychny, V. Tselyaev, S. Kamerdzhiev, F. Grummer, S. Krewald, J. Speth, A. Avdeenkov, and E. Litvinova, Phys. Lett. B **647**, 104 (2007).
[27] U. Kneissl, N. Pietralla, and A. Zilges, J. Phys. G **32**, R217 (2006).
[28] F. Ajzenberg-Selove, Nucl. Phys. A **506**, 1 (1990).
[29] F. R. Metzger, Prog. Nucl. Phys. **7**, 54 (1959).
[30] S. Agostinelli *et al.*, Nucl. Instrum. Methods A **506**, 250 (2003).

[31] S. Carson *et al.*, Nucl. Instrum. Methods A **618**, 190 (2010).
[32] N. Pietralla *et al.*, Phys. Rev. Lett. **88**, 012502 (2001).
[33] D. Savran *et al.*, Phys. Rev. C **71**, 034304 (2005).
[34] A. P. Tonchev, S. L. Hammond, J. H. Kelley, E. Kwan, H. Lenske, G. Rusev, W. Tornow, and N. Tsoneva, Phys. Rev. Lett. **104**, 072501 (2010).
[35] L. W. Fagg and S. S. Hanna, Rev. Mod. Phys. **31**, 711 (1959).
[36] J. A. Cameron and B. Singh, Nucl. Data Sheets **88**, 299 (1999).
[37] D. Savran *et al.*, Nucl. Instrum. Methods A **613**, 232 (2010).
[38] D. Savran, A. M. van den Berg, M. N. Harakeh, K. Ramspeck, H. J. Wörtche, and A. Zilges, Nucl. Instrum. Methods A **564**, 267 (2006).
[39] D. Savran, M. Babilon, A. M. van den Berg, M. N. Harakeh, J. Hasper, A. Matic, H. J. Wörtche, and A. Zilges, Phys. Rev. Lett. **97**, 172502 (2006).
[40] J. Endres, D. Savran, A. M. van den Berg, P. Dendooven, M. Fritzsche, M. N. Harakeh, J. Hasper, H. J. Wörtche, and A. Zilges, Phys. Rev. C **80**, 034302 (2009).
[41] J. Endres *et al.*, Phys. Rev. Lett. **105**, 212503 (2010).
[42] J. Endres (private communication).